<Modelling Properties of Steels during Solidification> ***<Edited by…>***
Materials Science and Technology (MS&T), 2006

Modelling of High Temperature Mechanical Properties and Density Change of Steels during Solidification

Z. Guo, N. Saunders, A.P. Miodownik and J.-Ph. Schillé

Sente Software Ltd., Surrey Technology Centre, Guildford GU2 7YG, U.K.

Keywords: Mechanical properties, density, steel, solidification, modelling

Abstract

A computer model has been created to calculate the high temperature mechanical properties and density change of steels during solidification. Such calculations were based on accurate thermodynamic description of the phase evolution, including changes in phase fraction and element concentration as a function of temperature and steel composition during the solidification process. The properties of each phase were firstly calculated based on its composition and temperature. Then the strength and density of the overall material were calculated via a mixture law. Results show that the calculated tensile strength and density values are in good agreement with experimental results in liquid, δ-ferrite, and γ-austenite single phase regions and mixed phase regions. The computer model is designed in such a way that all the calculations can be done automatically via a user friendly graphical interface when the alloy composition is given.

Introduction

Many researchers have studied high temperature mechanical properties because these are necessary for the prediction and control of stresses in the solidified shell of steel castings.(1,2) Density is another important factor required to optimise the conditions for continuous casting and any simulation of heat-conduction, solidification, elast-plastic deformation and fluid flow in many processes.(3,4) Recently, Mizukami and co-workers attempted to formulate quantitative relationships for the calculation of tensile strength and density based on alloy composition and the phases existing during the solidification process.(5,6,7) A brief description of their approach is given below using density as an example. First, thermodynamic calculation was used to calculate the phase fraction as a function of temperature during solidification. Then linear regression analysis was carried out to correlate the density of each phase with the temperature difference ΔT from a characteristic temperature (e.g. liquidus for the liquid phase) through optimisation against experimental measurements. Finally a linear mixture law was applied to obtain the overall density based on that of each phase. Although such models showed good agreement with their experimental data for both density and strength, the fact that no composition dependency was considered for the properties of each phase significantly limited its application to steel types outside the studied composition region. Their assumption that "the density of a phase has almost the same value when ΔT is the same" may be reasonable for the steels studied in their work, i.e. carbon steels with $Si+Mn \leq 1.06$ wt%, it would not be applicable to alloy steels. Also such calculation cannot be done easily for new alloys as the models require inputs such as phase fraction, solidus (T_S) and liquidus (T_L) temperatures that are not readily known for new alloys.

This paper reports our recent development of material models for the calculation of the density change and high temperature strength during solidification of steels. The present models have taken the dependency of density and strength on phase composition into account and therefore can be applied to steels of a wide composition range instead of just carbon steels. Many other important physical and thermophysical properties necessary for process modelling can be calculated as well, such as thermal expansion coefficient and Young's modulus. For the case of strength calculation, the effect of strain rate on flow stress is predicted, as is also the composition dependence. The major advantage of the present approach is that it is far less costly and has produced calculations within useful accuracy.

The first part of the paper describes the model development for the calculation of density and high temperature strength. The second part features the application of these models to the alloys studied by Mizukami et al. It should be noted that development of the present models had been completed well before the authors became aware of the work by Mizukami et al. and their data are used here solely for the purpose of testing the performance of the present models.

Experimental Details

The alloys studied are classified into two groups. The first group are Fe–C binary steel samples, Table 1; and the second group are Fe-based samples with alloying elements, Table 2. The steel ingots were produced using electrolytic iron and alloying elements in a vacuum furnace, and then were hot forged at a temperature of 1473 K. Some details of the experimental testing are explained below, whereas full details can be obtained from Refs. 5 and 6.

Table 1. Chemical composition of the Fe-C binary alloys (wt%)

Alloy	C	Si	Mn	P	S	Fe
FE00	0.005	<0.01	<0.01	<0.001	0.001	Bal.
FE04	0.039	<0.01	<0.01	<0.001	0.001	Bal.
FE08	0.079	<0.01	<0.01	<0.001	<0.001	Bal.
FE10	0.097	<0.01	<0.01	<0.001	<0.001	Bal.
FE14	0.14	<0.01	<0.01	<0.001	<0.001	Bal.
FE18	0.18	<0.01	<0.01	<0.001	0.001	Bal.
FE28	0.28	<0.01	<0.01	<0.001	0.001	Bal.
FE56	0.56	<0.01	<0.01	<0.001	0.001	Bal.

Table 2. Chemical composition of the steels with alloying elements (wt%)

Alloy	C	Si	Mn	P	S	Fe
ULC	0.005	0.01	0.12	0.014	0.0028	Bal.
LC	0.04	0.04	0.19	0.026	0.006	Bal.
MC1	0.11	0.10	0.48	0.020	0.008	Bal.
MC2	0.14	0.16	0.54	0.016	0.003	Bal.
HC	0.55	0.15	0.91	0.021	0.001	Bal.

All the alloys listed in Tables 1 and 2 were used for density measurement. The density was measured by a sessile drop profile method. It was carried out under heating conditions to avoid the influence from undercooling and cavities. The heating rate of the sample changed with temperature, being 0.21 K/s for the temperature range from room temperature to 1400 K and 0.083 K/s for the range from 1400 to 1973

K. Density measurements were carried out after 120s holding at a given temperature.

The alloys used for tensile testing include all the alloys in Table 1 and alloy MC1 in Table 2. The sample size was $1x10^{-2}$ m in diameter and $1x10^{-1}$ m in length. The centre region of $5x10^{-3}$ m in length of the sample was melted by high frequency induction heating. The temperature of the molten zone was raised from room temperature to 30 K below solidus temperature T_S and held for 30s, then the temperature was raised to 30 K above liquidus temperature T_L and held for 120s to keep the steady state. Afterwards, the sample was cooled at 0.17 K/s. The strain rate of the tensile test was $1x10^{-2}$ /s.

Model Development

The first step is to obtain the information on phase fraction and composition as a function of temperature through thermodynamic calculation. Then the models used to calculate the physical and thermophysical properties (e.g. density) and high temperature strength are described in details.

Phase evolution during solidification

The solidification of carbon steels changes with carbon content according to the equilibrium phase diagram. The primary phase during solidification is either δ phase or γ phase. Then solidification is completed either as a single phase or as two phases where δ/γ transformation occurs. It is the change of phase constituents during solidification that results in the changes in the deformation behaviour and density of the carbon steels. Figs. 1(a)–1(h) show the relationship between the L, δ or γ phase fraction and temperature given by equilibrium thermodynamic calculation for alloys listed in Table 1.[8] As for alloys in Table 2, their plots are essentially similar to that of the binary alloy with similar amount of carbon. The calculation was carried out using JMatPro®,[9)] which has been developed for the calculation of materials properties for the different phases present in multi-component alloys.

Fig. 1(a) shows the relationship between phase fraction and temperature for sample FE00. The primary phase of this sample during solidification is the δ phase and δ/γ transformation completes immediately at solidus temperature, and then the γ single phase is formed. When temperature decreases, the α phase is precipitated in the γ phase and the structure becomes α single phase. Figs. 1(b) and 1(c) show the change of phase fraction with temperature for FE04 and FE08 respectively. The primary phase of these two samples during solidification is the δ phase and the phase just after solidification remains a single δ phase. The γ phase formation starts after solidification completes. Its fraction increases with decreasing temperature, whereas the δ phase fraction approaches zero. After precipitation of the α phase, the γ phase fraction decreases and the α phase fraction increases.

Figs. 1(d) and 1(e) show the relationship between phase fraction and temperature for samples FE10 and FE14, respectively. Though the primary phase of these samples during solidification is the δ phase, the same as samples FE00–FE08, no single δ phase is formed at the end of solidification but a mixture of δ+γ phases. After the δ/γ phase transformation starts, the γ phase fraction increases with decreasing temperature and the δ phase fraction decreases. Figs. 1(f) and 1(g) show the change of phase fraction with temperature for samples FE18 and FE28, respectively. The primary phase of these samples is again the δ phase. However, its fraction shows a maximum value during solidification and disappears before solidification completes. After the γ phase precipitating, the (L+γ) phase structure forms and the structure becomes the γ single phase at solidus temperature. The γ/α transformation starts at low temperature in this experiment.

Fig. 1(h) shows the phase fraction vs. temperature for sample FE56. It differs from other samples in that the δ phase does not appear during solidification. The γ single phase forms at solidus temperature and the γ phase remains before the γ/α transformation begins.

Physical and thermophysical properties

This section describes the approach used for the calculation of density of multi-phase steels. The same approach can and indeed has been applied to many other physical and thermophysical properties, such as thermal conductivity and Young's modulus.10) Before being able to calculate the overall properties of a multi-phase system, one needs to know the properties of each individual phase. For each individual phase in a multi-component system, its properties are calculated using simple pair-wise mixture models.

$$P = \sum_i x_i P_i^0 + \sum_i \sum_{j>i} x_i x_j \sum_v \Omega_{ij}^v (x_i - x_j)^v \tag{1}$$

where P is the property of the phase, P_i^0 is the property of the phase in the pure element, Ω_{ij}^v is a binary interaction parameter dependent on the value of v, x_i and x_j are the mole fractions of elements i and j in the phase. Both P_i^0 and Ω_{ij}^v are temperature dependent. It is possible to include ternary or higher order effects where appropriate.

Once the property of each individual phase is defined, it will be linked to the phase transformation calculations described in the previous section. The property of the alloy can then be calculated using mixture models that can account for the effect of microstructure on the final property.11,12) Such models, which were developed for two-phase systems, have been extended to allow calculations to be made for multiphase structures.13) An extensive database has been created during the development of JMatPro for the calculation of physical and thermophysical properties of various phases in Al, Fe, Mg, Ni, and Ti alloys. Such databases have been extensively validated against experimental measurements.14) It is not the intention of this paper to give a full detailed account of how this has been achieved. Interested readers can refer to relevant papers listed in Ref. 14.

High temperature strength

Deformation at the combination of temperature and strain rate in the present study is controlled by the creep of the material. There are three phases γ, δ and L involved during the solidification of the steels studied. Because the liquid phase offers no flow resistance and therefore does not contribute to the strength of the alloy, the strength of the alloys can be calculated from two phases effectively, i.e. the body-centred-cubic (BCC) δ-ferrite and face-centred-cubic (FCC) γ-austenite. The creep behaviour of these two phases is discussed below, respectively.

Many formulations have been proposed to calculate the secondary creep rates of FCC alloys,15,16,17,18). The present work uses a formulation for the secondary creep rate that takes the stacking fault energy (γ_{SFE}) explicitly into account.19) This approach was selected as it contains parameters that have an identifiable physical basis and which can be calculated self-consistently. The ruling equation is taken as:

$$\dot{\varepsilon}_\gamma = A_1 D \left(\frac{\gamma_{SFE}}{Gb} \right)^3 \left(\frac{\sigma}{E} \right)^4 \tag{2}$$

where $\dot{\varepsilon}_\gamma$ is the secondary creep rate of the γ phase, A_1 a material-dependent constant, D the diffusion coefficient, γ_{SFE} the stacking fault energy of the matrix, b the Burgers vector, and σ the applied stress. G and E are the shear and Young's modulus of the matrix at the creep temperature, respectively. The values of G, E and D can be self-consistently calculated using JMatPro.20) This leaves A_1 as the only fitting parameter, which was fitted against extensive experimental data.21)

The formulation for the calculation of the secondary creep rates of BCC alloys follows the equation below:22,23)

$$\dot{\varepsilon}_\delta = A_2 D_{eff}\left(\frac{GB}{RT}\right)\left(\frac{\sigma}{E}\right)^n \tag{3}$$

where $\dot{\varepsilon}_\delta$ stands for the secondary creep rate of the δ ferrite, A_2 a material-dependent constant. The value of n can take on a range of values and is 3 for ferrite. Again, A_2 is the only fitting parameter and was obtained through fitting against experimental work.21)

When the creep rates of the two phases are known, the deformation rate for the dual phase structure can be described by the following expression to a first approximation:

$$\dot{\varepsilon} = f_\delta \dot{\varepsilon}_\delta + f_\gamma \dot{\varepsilon}_\gamma \tag{4}$$

where f_δ and f_γ represents the fraction of the δ phase and γ phase, respectively, whereas $\dot{\varepsilon}$ is the overall deformation rate. For tensile testing, the deformation rate is a constant strain rate, which is 0.01 s^{-1} in the present study. Therefore stress σ is the only parameter to be determined because all the other parameters involved in Eqs. (2)~(4) are known. Its value can be solved numerically for the given $\dot{\varepsilon}$ value, which corresponds to the tensile strength values measured from experiments. It should be noted that Eq. 4 is not applicable when the creep of the two phases differ significantly, for which case the creep rate of the overall alloy can then be calculated using more complicated mixture models.11,12) This is also true when one calculates the total strength from the strength contribution from the solid γ and δ phases and that from the liquid.

Results and Discussions

The model developed for the calculation of physical and thermophysical properties has been applied to predict the density change for steels listed in Tables 1 and 2, and comparison plots are shown in Figs. 2 and 3, respectively. As can be seen good agreement between calculation and experimental data was achieved. However, there does seem to be a tendency for the calculated densities of γ to be underestimated at higher C levels. It would be possible to refine some of the parameters in Eq. 2 so as to achieve a better fitting with the experimental data of Mizukami et al. However, this then detrimentally affects calculated results in comparison to experimental work from other established sources with carbon up to 0.95 wt%.3,24) Having said this, even for the alloys containing the highest amount of carbon, FE56 and HC, the error is typically around 1% and no more than 2%, and should be more than adequate for use in further process modelling.

A major advantage of the present approach, in comparison to a mainly experimental method of developing models for steel solidification, is that it is far less costly and many other important physical and thermophysical properties necessary for process modelling can be calculated, such as thermal expansion coefficient, Young’s, bulk and shear modulii, Poisson’s ratio, thermal conductivity and diffusivity, electrical conductivity, viscosity, and resistivity.

The calculated high temperature strength for the steels listed in Table 1 and MC1 in Table 2 is shown in Figs. 4 and 5, respectively, in comparison with experimental data, where the agreement with the results of Mizukami et al. is generally good and within useful accuracy for alloy development and process modelling.

As for the thermo-physical and physical properties, an advantage of the present method is that substantially more information can be obtained. For the case of strength, principally the effect of strain rate on flow stress is predicted, as is also the composition dependence. The latter is particularly useful when considering steels other than the simple carbon and low alloy types studied by Mizukami et al..

The influence from dendrite arm spacing (DAS) on strength was not considered in the present model. In fact it was not considered in the original model by Mizukami et al. either. At first sight, such good agreement despite neglecting the influence of DAS can be surprising. However, the DAS effect on strength is very similar to the grain size effect, which may well be predominantly a low-temperature effect. When the temperature is high enough and the deformation is controlled by creep, such a size factor may not play a critical role on strength after all.

Summary

This paper describes the development of advanced computer models for the calculation of physical and thermophysical properties, such as density, and high temperature strength of steels. Such calculations were based on an accurate description of the phase evolution, including changes in phase fraction and element concentration as a function of temperature and steel composition linked to well tested material property models. The experimental work by Mizukami et al. has been used to test the performance of the models and results show that the calculated strength and density values are in good agreement with experimental results in liquid, δ-ferrite, and γ-austenite single phase regions and mixed phase regions. In comparison with previous work in these fields, the present modelling approach provides a cost-effective way of obtaining important material information for multi-component systems. The computer model is designed in such a way that all the calculations can be done automatically via a user friendly graphical interface when the alloy composition is given.

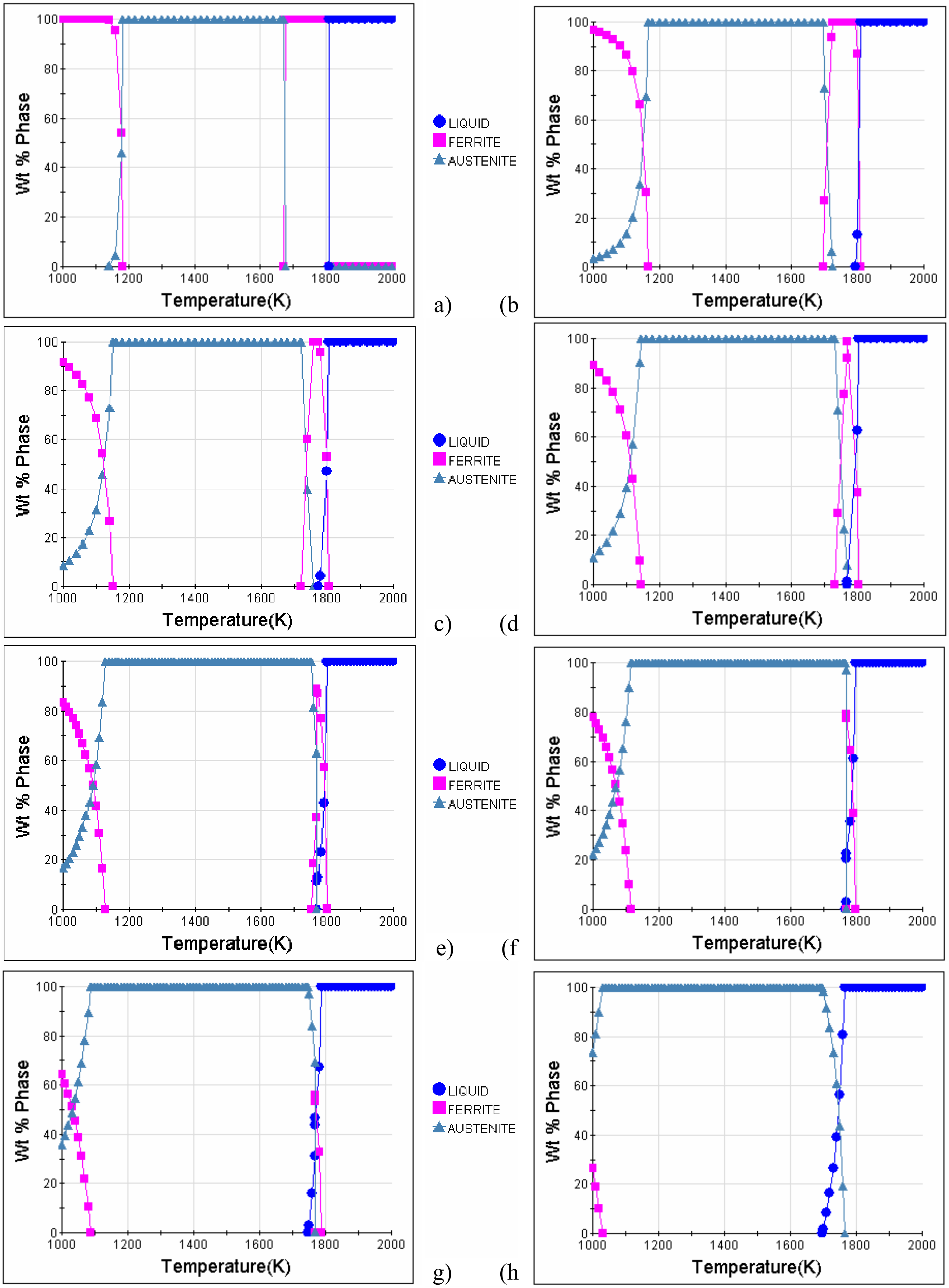

Figure 1. Change in fraction of phase with temperature for the steel samples studied:
(a) Fe00, (b) Fe04, (c) Fe08, (d) Fe10, (e) Fe14, (f) Fe18, (g) Fe28, and (h) Fe56

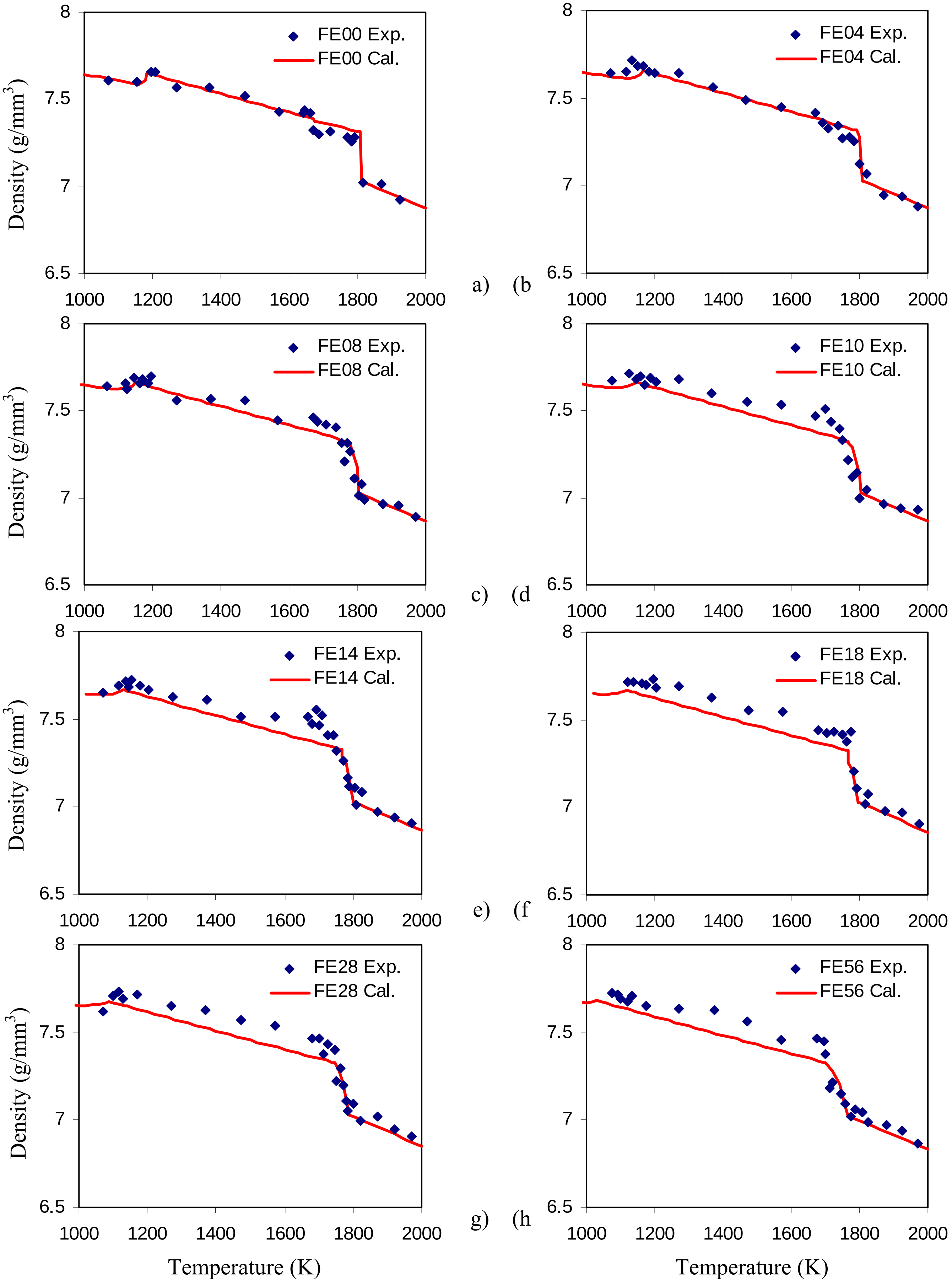

Fig. 2. Change in density for steels listed in Table 1, (a) Fe00, (b) Fe04, (c) Fe08, (d) Fe10, (e) Fe14, (f) Fe18, (g) Fe28, and (h) Fe56

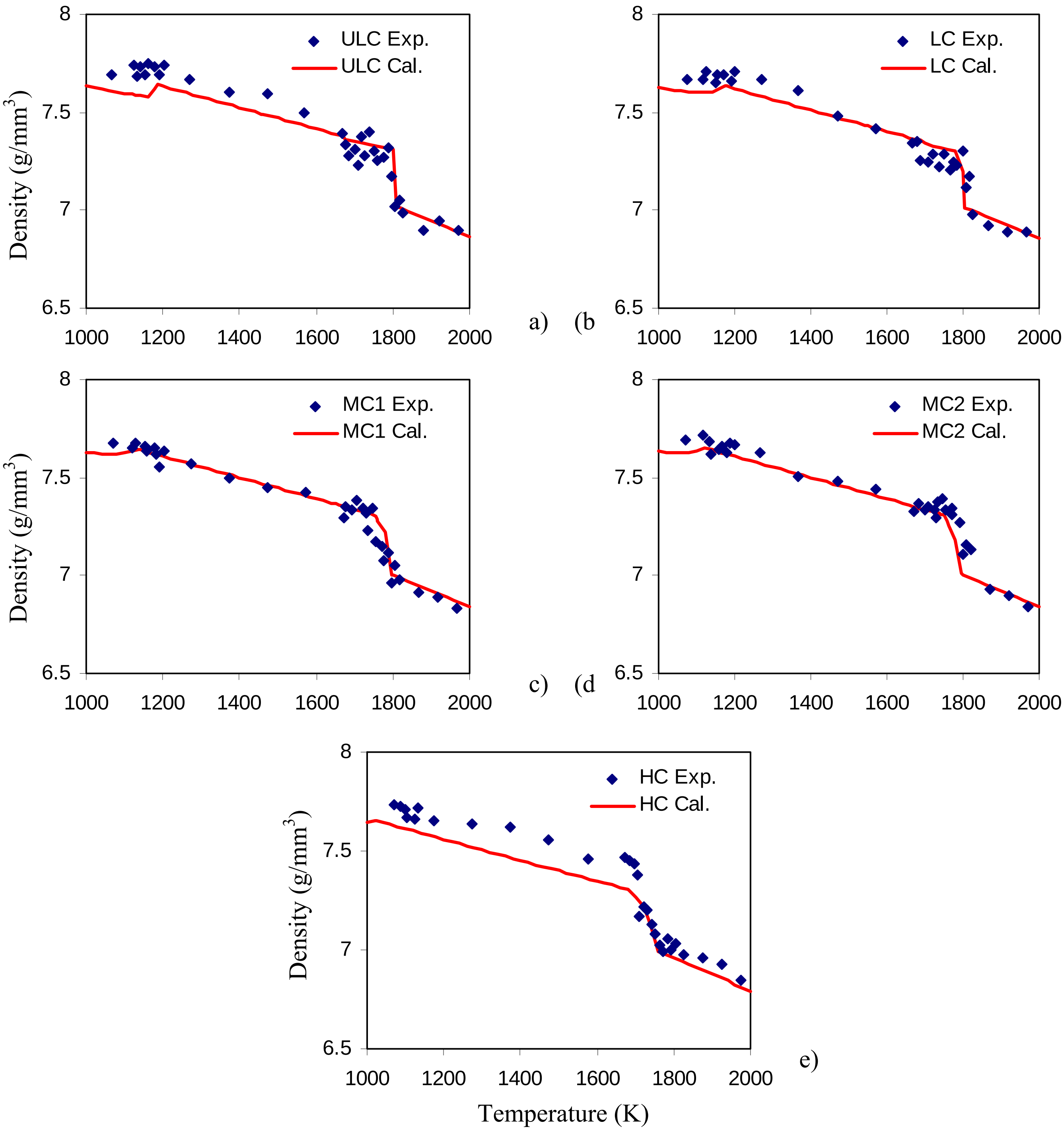

Fig. 3. Change in density for steels listed in Table 2, (a) ULC, (b) LC, (c) MC1, (d) MC2, and (e) HC

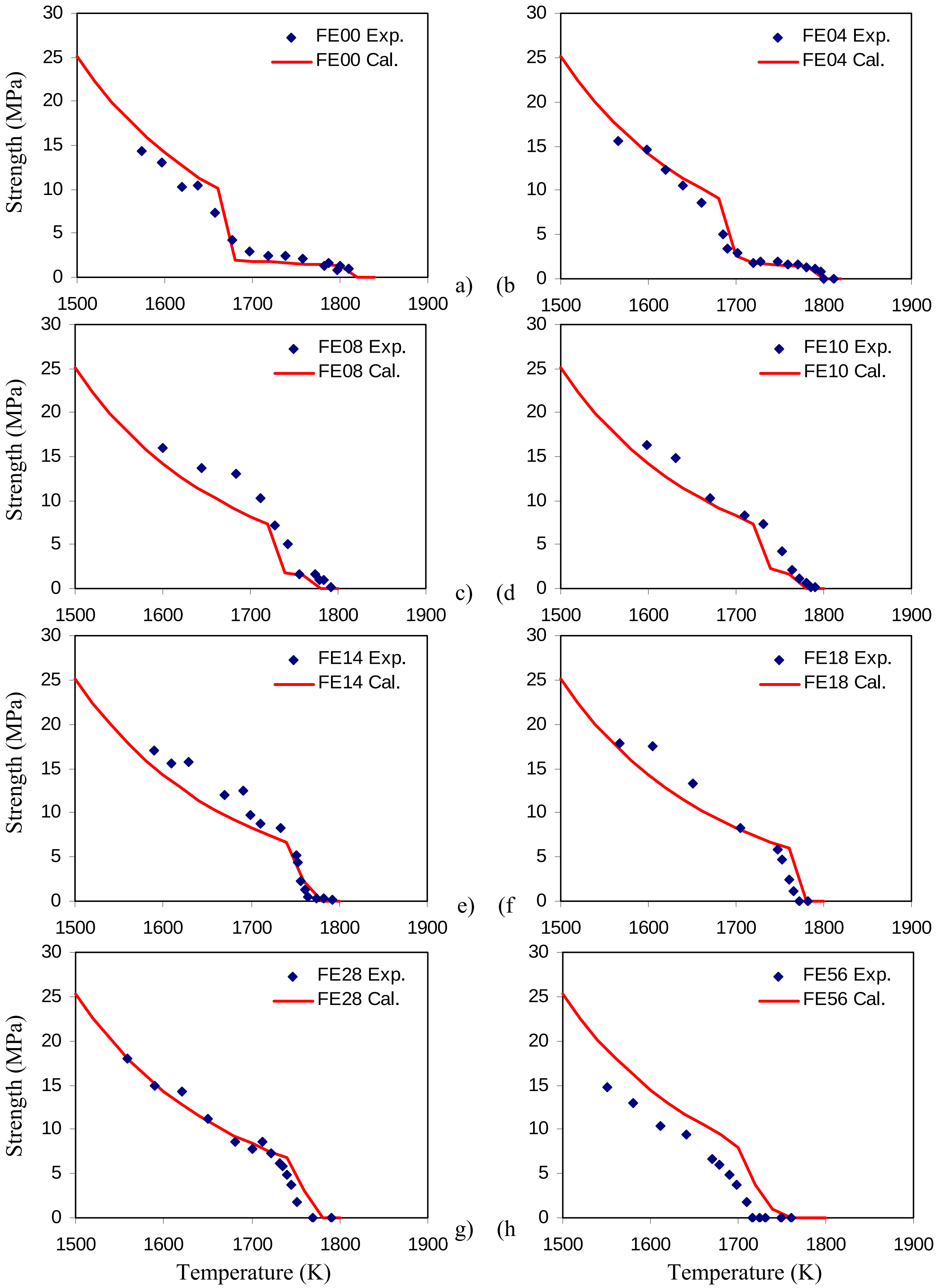

Fig. 4. Strength vs. temperature for steels in Table 1, (a) Fe00, (b) Fe04, (c) Fe08, (d) Fe10, (e) Fe14, (f) Fe18, (g) Fe28, and (h) Fe56

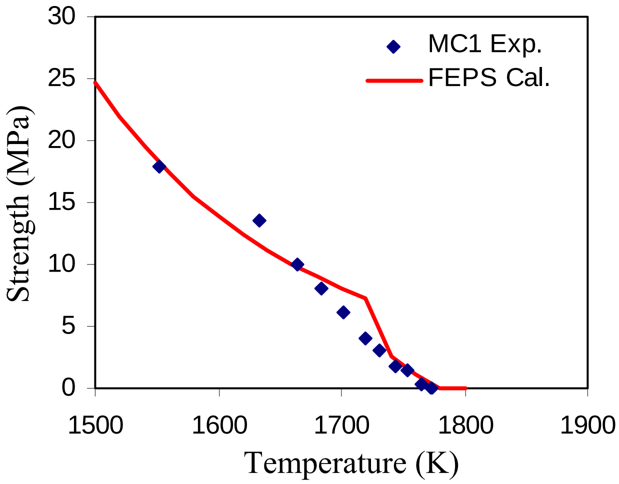

Fig. 5. Strength vs. temperature for MC1 steel

References:

---

1) W.T. Lankford Jr., *Metall. Trans.* **3** (1972) 1331
2) T. Nakagawa et al., *ISIJ International*, **35** (1995) 723–729
3) L.D. Lucas, *Mem. Sci. Rev. Met.*, **61** (1964) 97
4) P.J. Wray, *Metall. Trans.*, **5** (1974) 2602
5) H. Mizukami, A. Yamanaka and T. Watanabe, *ISIJ International*, **42** (2002) 964–973
6) H. Mizukami, A. Yamanaka and T. Watanabe, *ISIJ International*, **42** (2002) 375–384
7) H. Mizukami et al., *ISIJ International*, **40** (2000) 987–994
8) N. Saunders and A.P. Miodownik, CALPHAD – Calculation of Phase Diagrams, Pergamon Materials Series vol.1, (Ed.: R.W. Cahn), Elsevier Science, Oxford, **1998**
9) JMatPro®, Sente Software Ltd., Guildford GU2 7YG, U.K. 2001
10) Z. Guo et al., *Mater. Sci. Eng. A*, **413-414** (2005) 465-469
11) Z. Fan, P. Tsakiropoulos and A.P. Miodownik, *Mat. Sci. Technol.*, **8** (1992) 922-929
12) Z. Fan, *Phil. Mag. A*, **73** (1996) 1663-1684
13) A.P. Miodownik et al., unpublished research, Sente Software Ltd., Guildford GU2 7YG, U.K.
14) http://www.sentesoftware.co.uk/biblio.html (papers on JMatPro downloadable in pdf format)
15) B. Wilshire and H.E. Evans, Creep of Metals and Alloys, Inst. Metals, 1985
16) X.S. Xie et al., *Scripta Metall.*, **16** (1982) 483-488
17) H. Burt, J.P. Dennison and B. Wilshire, *Metal Science*, **13** (1979) 295
18) R. Lagneborg and B. Bergman, *Metal Science*, **10** (1976) 20
19) C.R. Barrett and O.D. Sherby, *Trans. Met. Soc. AIME*, **233** (1965) 1116-1119
20) N. Saunders et al., *JOM*, **55** (2003) 60-65
21) Z. Guo et al., unpublished research, Sente Software Ltd., Guildford GU2 7YG, U.K.
22) J. Koike et al., *Mater. Sci. Eng. A*, **213** (1996) 98-102
23) C. Schuh and D.C. Dunand, *Scripta Mater.*, **45** (2001) 1415-21
24) N. Ridley and H. Stuart, *Metal Science*, **4** (1970) 219